The Satellite Irrigation Management Support (SIMS) System User Documentation

December 9, 2018

Last updated March 3, 2021

Prepared by:

Forrest S. Melton[1,2], Lee F. Johnson[1,2], Alberto Guzman[1,2], Will Carrara[1,2], Conor Doherty[3]

[1] Cooperative for Research in Earth Science and Technology, NASA Ames Research Center, Moffett Field, CA

[2] School of Natural Sciences, California State University, Monterey Bay, Seaside, CA

[3]Stanford University, Stanford, CA, USA

Abbreviations

ET	Evapotranspiration
ET_a	Actual evapotranspiration calculated from ground measurements
$ET_{a\ eb}$	Actual evapotranspiration calculated using micrometeorological instrumentation and an energy balance approach
$ET_{a\ swb}$	Actual evapotranspiration calculated using a surface water balance approach
ET_c	Crop evapotranspiration
$ET_{c\text{-}SIMS}$	Estimated crop evapotranspiration from SIMS
$ET_{c\text{-}SIMS+}$	Estimated crop evapotranspiration from SIMS combined with a soil water balance model
ET_o	Grass reference evapotranspiration
f_c	Fractional cover
h	Crop height
K_{cb}	Basal crop coefficient
K_d	Density coefficient
K_e	Evaporation coefficient
K_s	Stress coefficient
MAD	Mean Absolute Difference
MAE	Mean Absolute Error
MBE	Mean Bias Error
NDVI	Normalized Difference Vegetation Index
NIR	Near-infrared
RMSE	Root Mean Square Error
SIMS	Satellite Irrigation Management Support system
S2	Sentinel-2 satellites (2A and 2B)

1. Introduction

This document describes the algorithms and equations implemented within the NASA Satellite Irrigation Management Support (SIMS) System. SIMS was developed to support satellite mapping of crop coefficients and evapotranspiration (ET) from irrigated lands and increase access to this data for agricultural producers and water resource managers. Satellite data offers a cost-effective means of mapping crop coefficients and monitoring ET over large areas, and multiple approaches have been developed over the past two decades. The SIMS software repositories are available as open source code and include python implementations of SIMS for use on desktop computers, high performance computing environments, and Google Earth Engine. The SIMS software repositories are available at: https://github.com/guzman2319/pySIMS For information on the SIMS Application Program Interface (API), please see: http://sims.et/documentation

SIMS used surface reflectances from multiple satellites as inputs to the algorithms described below. Reflectance-based approaches for calculation of crop coefficients have been employed since at least the 1980s, when weighing lysimeters and spectral vegetation indices were used to develop crop coefficients for corn (Bausch and Neale, 1987; Neale et al., 1990), and a recent review of these methods is provided by Pôças et al. (2020). Such approaches employ empirically derived relationships among vegetation indices (VIs), actual crop ET measured in the field with a weighing lysimeter or other instrumentation, and the meteorologically driven reference ET to calculate crop coefficients.

The primary strength of reflectance-based approaches is that the relationships between the VIs and the crop coefficients are readily calculated and can be efficiently calibrated, making these approaches straightforward to automate. A second key strength is that the red, near-infrared (NIR), and blue bands used to calculate these vegetation indices are available at field scale from the multispectral instruments on multiple satellite platforms, increasing the temporal frequency of the satellite observations needed to drive the models, and reducing dependency on a single satellite. Taken together, when combined with provisional atmospheric correction, these attributes suggest that there is good potential for reflectance-based models to operate with minimal latency to support irrigation management applications. The third primary strength is that, relative to variables like land surface temperature, the VIs tend to change more gradually on daily to weekly timescales, reducing sensitivity to the time of satellite overpass or the frequency of irrigation events.

One limitation of reflectance-based approaches is that the field studies used to develop the relationships between VIs and crop coefficients are conducted for well-watered (i.e., non-water stressed) conditions at different growth stages, making the approach less sensitive to intermittent water stress, or deficit irrigation that is not sufficient to affect the crop canopy. Additionally, they are less sensitive to soil evaporation. As a result, they typically require use of a soil water balance model to correct for soil evaporation, especially over bare soil and early during the crop growth cycle when fractional crop cover is low. A further limitation is that crop coefficients have less utility outside of irrigated agriculture. However, ongoing work is developing relationships and techniques that would facilitate the application of this approach to a range of other landscape types (Glenn et al., 2011; Nagler et al., 2013; Beamer et al., 2013).

The SIMS framework (Melton et al., 2012; Pereira et al., 2020) integrates satellite data with grass reference ET (ET_o) information from the California Department of Water Resources (CDWR) California Irrigation Management Information System (CIMIS) and gridMET to map crop canopy development and key measures of crop water requirements at the scale of individual fields. SIMS uses a reflectance-based (visible, NIR) approach developed mainly to inform irrigation management strategies and advance on-farm water use efficiency. SIMS was originally developed through a partnership between NASA, California State University Monterey Bay (CSUMB), and the California Department of Water Resources (CDWR) to increase access to satellite data for use in irrigation scheduling and regional water accounting. SIMS data products are produced at a spatial scale of 30m x 30m (0.22 acres) and include the normalized difference vegetation index (NDVI), crop fractional cover (f_c), basal crop coefficients (K_{cb}) and crop evapotranspiration ($ET_{c\text{-}SIMS}$). NDVI, f_c and K_{cb} data are updated with each satellite overpass (currently every eight days), and $ET_{c\text{-}SIMS}$ data are updated daily through integration of ET_o data from CIMIS. $ET_{c\text{-}SIMS}$ is calculated as the product of K_{cb} and ET_o, and provides a simplified measure of crop ET that excludes the contributions of evaporation from exposed soil, or crop water stress that does not manifest as growth reduction.

2. Software availability and integration with other tools

SIMS software is available both as a python-based application for desktop computers and as an implementation on Google's Earth Engine platform (Gorelick et al., 2017) that uses the Earth Engine python application programming interface. SIMS software is released under the Apache 2.0 and Creative Commons by Attribution 4.0 licenses, and available for download via open source software repositories on github at https://github.com/Open-ET/openet-sims-beta. An API is also

available for the Earth Engine implementation to facilitate machine to machine access and integration of data from SIMS with other applications (Guzman et al., 2018).

While ET data are valuable for managing irrigation to match crop water requirements and minimize both unintentional leaching and unintentional deficit irrigation, the majority of growers and irrigators will find ET data most useful when it is converted to irrigation system run-times. Incorporation of satellite data into existing irrigation and nutrient management software applications is an effective approach to increase uptake and adoption of remote sensing as a tool to enhance irrigation scheduling and advance on-farm water use efficiency. The API facilitates integration of SIMS data into third-party irrigation and nutrient management software applications. This interface has been successfully used by applications including CropManage and IrriQuest (Cahn and Johnson, 2018) and is available for use by other tools. Using the API, these applications can access SIMS f_c, K_{cb}, and $ET_{c\text{-}SIMS}$ for locations or regions of interest, specify the crop type and crop height as input to the SIMS calculations, and retrieve data for any time period of interest from 2003 to present. Data is returned in text formats including comma separate values (csv) and geojson.

3. Cautions and limitations

SIMS was developed primarily to enhance the use of satellite data for irrigation management, and data are freely available via the SIMS API. For operational use in irrigation management, users are encouraged to modify irrigation practices gradually. Use of soil moisture sensors and flow meters in combination with remotely sensed estimates of $ET_{c\text{-}SIMS}$ are encouraged to provide the most complete and accurate overall assessment of irrigation management. For water accounting

and reporting purposes, as well as regional ET mapping applications, users are encouraged to account for soil evaporation and crop water stress, as needed, via use of a soil water model or joint use of SIMS in combination with an energy balance approach such as METRIC (Allen et al., 2007), DisALEXI (Cammalleri et al., 2013), or SSEBop (Senay et al., 2013). At minimum, the accuracy of $ET_{c\text{-}SIMS}$ data relative to the ground-based ET datasets should be applied to data from SIMS to account for the possible range in actual ET.

4. Satellite Data and Methods

4.1 Satellite Data

SIMS utilizes satellite observations in the red and NIR wavelengths to derive NDVI as:

$$\text{NDVI} = \frac{\rho_{nir} - \rho_{red}}{\rho_{nir} + \rho_{red}} \quad (1)$$

Where ρ_{nir} and ρ_{red} are surface reflectance in the NIR and red wavelengths, respectively. NDVI is a widely used remote sensing index that provides a unitless measure of vegetation density and condition that ranges from -1 to 1 (Goward et al., 1991). SIMS is currently driven by data from Landsat and Sentinel-2, with potential for augmentation by SPOT, Rapideye and other satellite platforms that provide data in the red and NIR wavelengths. SIMS can use both top-of-atmosphere (TOA) reflectances and atmospherically corrected surface reflectance values, though use of surface reflectances generally leads to greater accuracy. For the comparisons with ground-based ET datasets described below, atmospherically corrected surface reflectance data were obtained from the USGS Landsat Collection 1 for Thematic Mapper (TM) on Landsat 5, the Enhanced Thematic Mapper (ETM+) on Landsat 7, and the Operational Land Imager (OLI) on Landsat 8. Data were screened using quality assurance (QA) and cloud mask data included with each Landsat L1T file, and the best available observation for each 8-day period was selected for

each pixel. In cases where multiple cloud-free, high-quality observations were available within an 8-day period, Landsat 8 was given priority, or the most recent scene was used in cases where overlap between two Landsat 8 scenes provided more than one value per pixel for each 8-day period. Using the python-based implementation, or the open source software implementation on Earth Engine, SIMS can also be run using data for individual overpass satellite overpass dates from all available cloud-free Landsat and Sentinel-2 scenes.

4.2 Calculation of fractional cover values from satellite data

SIMS incorporates the density coefficient described by Allen and Pereira (2009) to calculate crop coefficients from satellite data. The use of the Allen and Pereira density coefficient approach to compute basal crop coefficients and ET_c using direct in-field observations of f_c and h was recently tested by Pereira et al. (2020) for a variety of crops. The study included comparisons with soil water balance and lysimeter ET observations and confirmed the overall robustness of the approach. To parameterize the density coefficient approach in support of wide-area mapping of crop coefficients via remote sensing, SIMS first converts satellite NDVI to f_c based on an empirically derived equation developed by USDA in collaboration with NASA:

$$f_c = 1.26 * NDVI - 0.18 \quad (2)$$

Where, f_c is the crop fractional cover and NDVI is the normalized difference vegetation index. Johnson & Trout (2012) and Trout et al. (2008) found robust relationships between NDVI and f_c across a range of different crop types and canopy architectures. Eq. 2 was derived based on in-situ f_c measurements of 49 commercial fields and 18 major crop types (row crops, grains, orchard, vineyard) of varying maturity that were made on 11 Landsat overpass dates in the San Joaquin Valley from April to October 2008. Landsat L1T terrain-corrected images were

transformed to surface reflectance and converted to NDVI. A strong linear relationship between NDVI and f_c (r^2 = 0.96, RMSE = 0.062) was reported.

4.3 Deriving crop coefficients from satellite data via the density coefficient approach

The basal crop coefficient, K_{cb}, represents transpiration and diffuse evaporation, and can be described as "primarily the transpiration component of ET and a small evaporation component from soil that is visibly dry at the surface" (Allen et al., 1998). K_{cb} can be estimated for standard climate conditions by a density coefficient (K_d) derived from a simple biophysical description of the canopy involving the effective fraction of ground covered or shaded by vegetation ($f_{c\ eff}$), crop height (h), and also considering a stomatal control factor (ASABE, 2007; Allen and Pereira, 2009; ASCE, 2015; Pereira et al., 2020). K_d links increases in K_{cb} to increasing vegetation amount and is calculated following Allen and Pereira (2009), Eq. (10) as:

$$K_d = \min(1, M_L * f_{c\ eff}, f_{c\ eff}^{1/(1+h)}) \quad (3)$$

Where M_L is a multiplier "describing the effect of canopy density on shading and on maximum relative ET per fraction of ground shaded" (Allen and Pereira, 2009). M_L is assigned a value 2 for annuals and, with some exception, 1.5 for perennials (trees and vines). For use within the SIMS framework, no distinction is made between $f_{c\ eff}$ and f_c, which is the fraction of surface covered by green vegetation as measured from directly overhead, and the latter notation is used henceforth.

Maximum crop height (h_{max}) in meters is listed by Table 12 of Allen et al. (1998) for several crop types. An estimation strategy is needed to support remote sensing or other cases where h cannot be directly measured. For annuals, it is here assumed that h starts at zero and

increases linearly with f_c to a plateau value of h_{max} at 0.7 f_c, generally regarded as effective full cover:

$$h = h_{max} * (\min (f_c / 0.7, 1)) \quad (4a)$$

Crop height for vineyards and mature orchards is set to h_{max}:

$$h = h_{max} \quad (4b)$$

An immaturity correction is implemented for orchards when $f_c < 0.5$ (after Table 5 of Allen and Pereira, 2009), such that:

$$h = h_{max} - 1 \quad (4c)$$

No immaturity correction is applied to vineyards, where h is typically set by physical trellis configuration and young vineyards are thus the same height as more mature plantings.

$K_{cb\ full}$, which represents conditions at peak plant growth for conditions having nearly full ground cover, is calculated as a simplified version of Eq. 7a of Allen and Pereira (2009):

$$K_{cb\ full} = F_r * (\min(1.0 + 0.1h_{max}, 1.2)) \quad (5)$$

Where F_r (range 0-1) is an adjustment factor related to stomatal regulation. For annuals, F_r is assigned a standard value of 1. For perennials, which tend to exhibit more stomatal control on transpiration, F_r is < 1 and varies by crop type (Allen and Pereira, 2009; Pereira et al., 2020). Further, initial and mid-season F_r in perennials generally exceeds the end-of-season value. To account for this exceedance, Table 11 from Allen et al. (1998) is used to specify the date range of the late-season stage, and a linear interpolation is applied between mid-season and end-of-season F_r as a function of the day of year. Eq. (5) assumes standard climate, and thus excludes wind speed and relative humidity corrections.

Finally, K_{cb} is derived following Eq. (5a) from Allen and Pereira (2009):

$$K_{cb} = K_{cb\ min} + K_d * (K_{cb\ full} - K_{cb\ min}) \quad (6)$$

Where $K_{cb\ min}$ is set to 0.15, which is the minimum K_{cb} value for bare soil under typical agricultural conditions (Allen and Pereira, 2009).

The parameter values per crop used to enable calculations in Eqs. (2) through (6) are provided primarily by Table 1 and Table 2 of Allen and Pereira (2009). Values of h_{max} for annual crops are drawn from Table 12 of FAO56 (Allen et al., 1998). Values from Table 11 of FAO56 are used for the late stage start and stop dates. Fig. 1 shows the f_c-K_d response curve and Fig. 2 shows the f_c-K_{cb} response curve for perennials during the initial and mid-season stages. These figures are extrapolated through the full theoretical range of f_c values, and f_c values at the upper end of the range may not be observed under standard agronomic practices for some crops (e.g., wine grapes). Annuals are not plotted individually due to a large number of annual crops, but Fig. 3 shows class averages based on mean class h_{max} as derived from crop h_{max} values. As height increases, leaf area, radiation capture, and turbulent exchange also tend to increase (Allen and Pereira, 2009; Allen et al., 1998). In both cases, it is seen that per Eq. (3), the K_d distribution at a given f_c is positively related to h, with M_L also playing a role in perennials at low-to-intermediate cover (see apple/cherry/pear and avocado). The K_{cb} distributions are driven by differences in $K_{cb\ full}$, with pronounced effect in perennials due to F_r (stomatal control) variation.

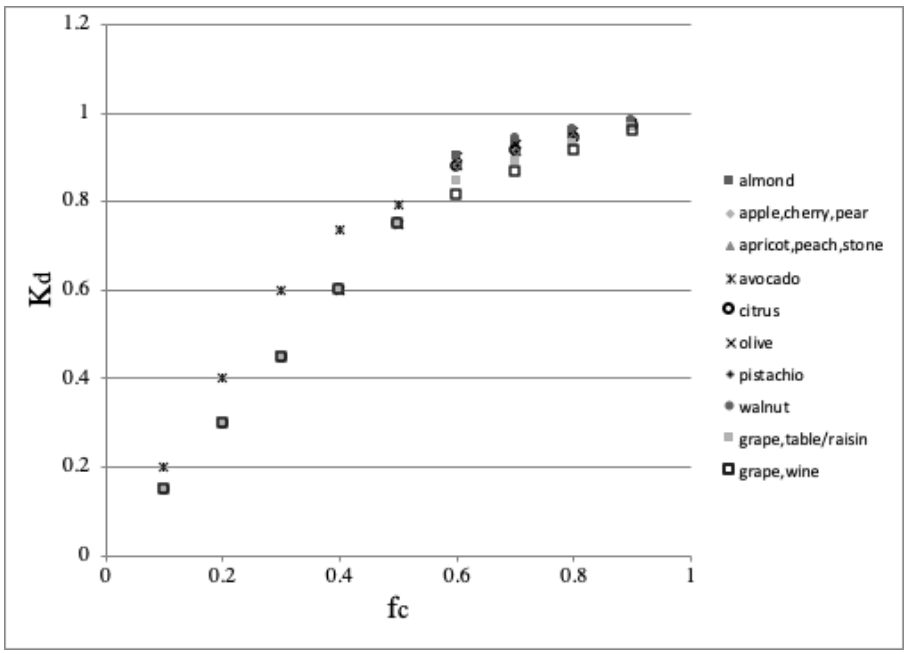

Fig. 1. Relationship between f_c and K_d for perennials during initial through mid-season stages. Data calculated for perennial crops for f_c values from 0-1 following Allen and Pereira (2009).

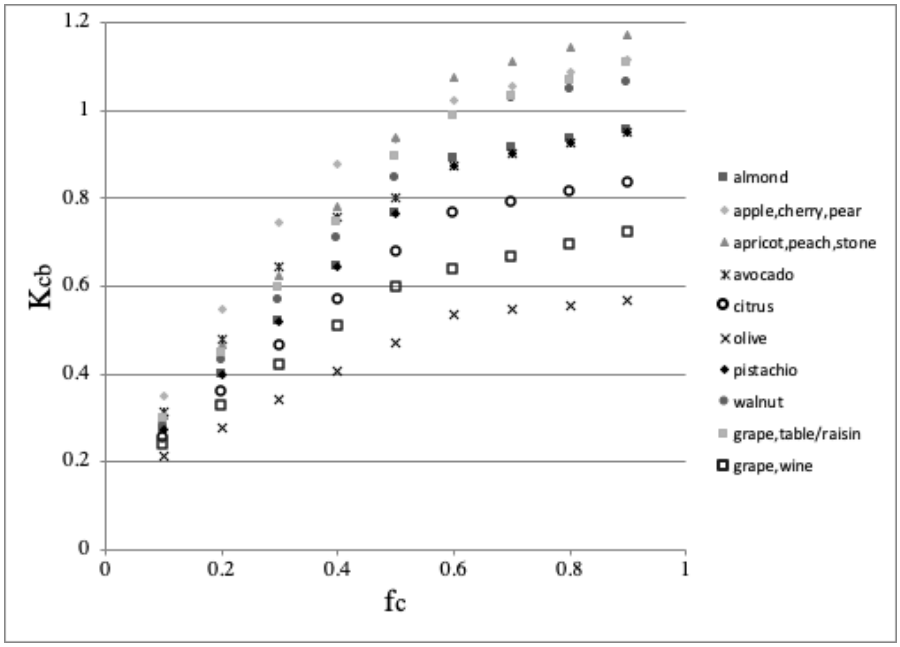

Fig. 2. Relationship between f_c and K_{cb} for perennials during initial through mid-season stages. Data calculated for perennial crops for f_c values from 0-1 following Allen and Pereira (2009).

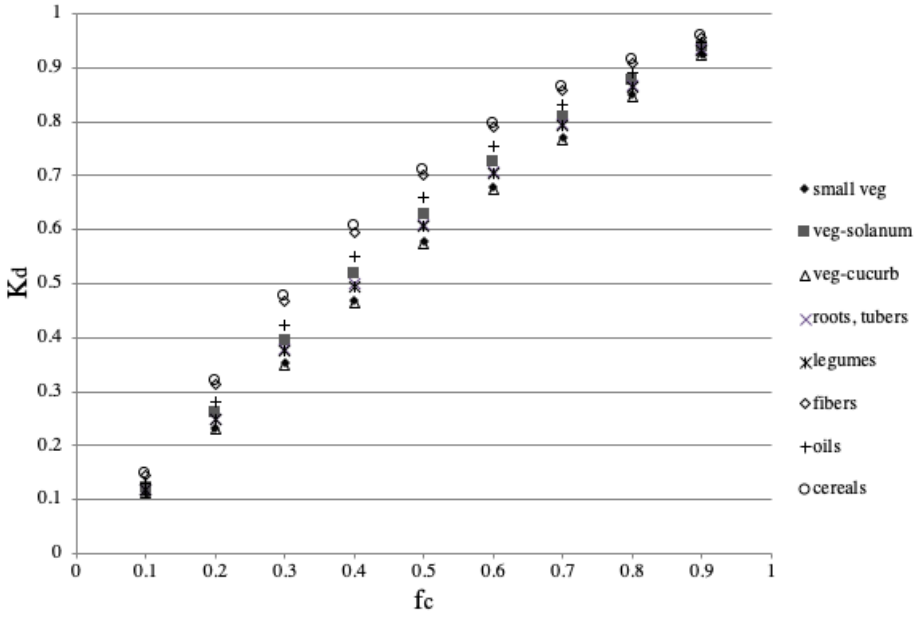

Fig. 3a. Relationship between f_c and K_d for annual crop classes. Data calculated for representative annual crops for f_c values from 0-1 following Allen and Pereira (2009).

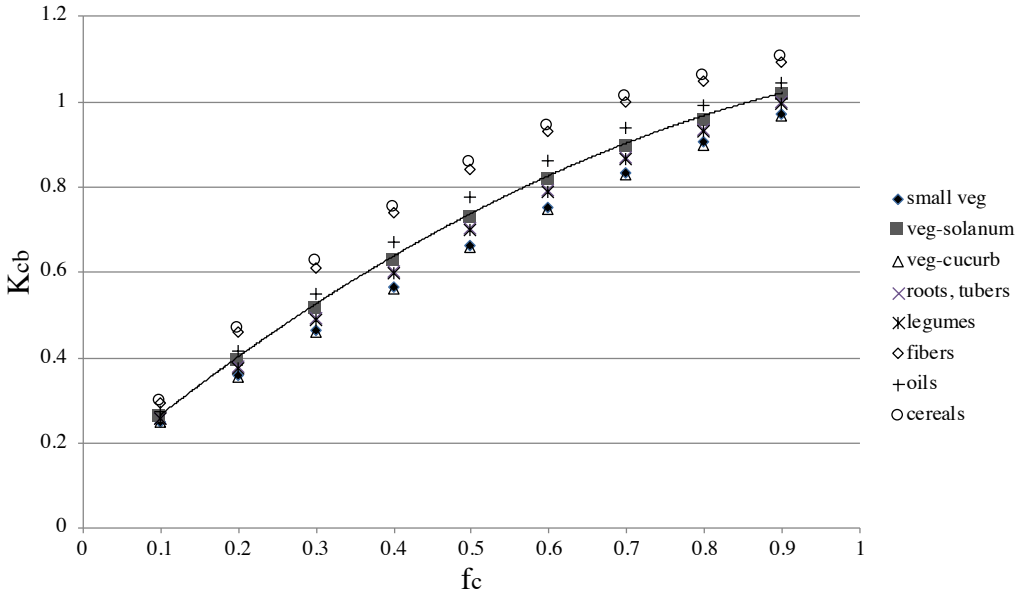

Fig. 3b. Relationship between f_c and K_{cb} for annual crop classes; trendline per Eq. 7. Data calculated for representative annual crops for f_c values from 0-1 following Allen and Pereira (2009).

4.4 Accounting for uncertainty in crop type

For field-scale irrigation scheduling and management applications, detailed crop type information can be provided reliably by the application user and relayed to SIMS via the API. For regional to national scale remote sensing applications, crop type information is updated less frequently and SIMS must address uncertainty in information on crop types. Perennial crops can be identified reasonably well through prior-year satellite-based crop maps available from the USDA National Agricultural Statistics Service (NASS) Cropland Data Layer (CDL) (Johnson and Mueller, 2010; Boryan et al., 2011) and county-level reporting records, as their spatial distribution can be assumed to be fairly constant from one year to the next. Thus, these crops are best evaluated on a crop-specific basis as above. Annuals are more problematic due to inconsistent seasonal planting patterns responding to market conditions, crop rotation practices, resource availability, and other considerations. Their spatial distribution is typically unknown until after end-of-season. A best-fit trendline for Fig. 3b can support K_{cb} estimation for real-time satellite surveys in cases where the annual crop type cannot be determined with high confidence as:

$$K_{cb} = -0.4771(f_c^2) + 1.4047(f_c) + 0.15 \quad (7)$$

An error analysis was conducted to compare estimated K_{cb} values for annual crops using Eq. (7) and K_{cb} values using crop-specific parameterizations for Eqs. 2-6. Results from this analysis found that the MAE in K_{cb} estimation, due to the use of Eq. (7) in place of crop-specific parameters for the density coefficient approach, ranges from 0.01-0.09 for the various annual crop classes, corresponding to an additional expected error in ET estimates of 0.07-0.65 mm/day for the Five Points vicinity of California's Central Valley during the annual period of peak

evaporative demand. Use of Eq. (7) was not required for the current study due to the availability of specific crop type information in all cases.

4.5 Calculation of crop evapotranspiration in SIMS

For ET mapping analyses conducted in California, and for the comparisons against ground-based observations presented here, SIMS ingests data from Spatial CIMIS, which produces daily maps of ET_o for California on a 2km statewide grid (Hart et al., 2009). K_{cb} values for each pixel are linearly interpolated to a daily timestep between Landsat overpasses. Combining SIMS K_{cb} with Spatial CIMIS ET_o data facilitates the daily estimation of $ET_{c\text{-}SIMS}$ following the FAO56 dual crop coefficient approach (Allen et al., 1998). However, due to the fact that reflectance-based approaches are less sensitive to evaporation from exposed soil, in Eq. (8), SIMS treats the soil evaporation coefficient (K_e) as equal to zero by default, unless K_e is calculated using a soil water balance model as described in Section 2.6.

$$ET_{c\text{-}SIMS} = (K_{cb} + K_e)ET_o \quad (8)$$

For applications in other states in the U.S., SIMS can also integrate ET_o data from gridMET (Abatzoglou, 2013) or reference ET from agricultural weather stations networks such as the U.S. Bureau of Reclamation AgriMet network, Nevada's NICE Net, Oklahoma's Mesonet, or the Automated Weather Data Network operated by the High Plains Regional Climate Center.

4.6 Calculation of Soil Evaporation and Stress Coefficients

At the scale of individual fields, a soil water balance model can be applied to correct $ET_{c\text{-}SIMS}$ values for the influence of crop water stress and evaporation from exposed soil. In this study, a soil water balance model based on the FAO56 approach (Allen et al., 1998) was used for

calculation of evaporation coefficients (K_e) and stress coefficients (K_s) for each site. This facilitated transformation of $ET_{c\text{-}SIMS}$ values to adjusted ET_c ($ET_{c\ adj}$) values following FAO56 Eq. (80), as:

$$ET_{c\ adj} = (K_s * K_{cb} + K_e)ET_o \quad (9)$$

$ET_{c\ adj}$ represents the potential crop ET adjusted for water stress, and provides an estimation of expected ET_a. In our analysis, we used the satellite-derived K_{cb} values from SIMS as an input to Eq. (9). To differentiate our results from the standard tabular approach described by FAO56 to calculate $ET_{c\ adj}$, we henceforth use $ET_{c\ SIMS+}$ to notate the ET_c values calculated using SIMS K_{cb} combined with the K_e and K_s values calculated using the soil water balance described below. K_e represents evaporation from the soil surface. K_e is at a maximum when the soil surface (evaporable layer) is wet, after irrigation or rainfall, and declines as the layer dries out and approaches zero when no water remains near the soil surface for evaporation. The evaporable zone depletion (D_e) is estimated at the start of the analysis period as:

$$D_e = 1000 * (\theta_{FC} - \theta_e) * Z_e \quad (10)$$

Where θ_{FC} is the water content at soil field capacity from Table 19 of FAO56 (Allen et al., 1998), θ_e is the initial water content of the evaporable zone, and Z_e is the depth of the evaporable zone (set to 0.1 m). θ_e is calculated as:

$$\theta_e = \theta_{FC} - \alpha*(\theta_{FC} - 0.5 * \theta_{WP}) \quad (11)$$

where α is an initial depletion factor based on data from soil moisture sensors.

To provide an upper limit on soil evaporation, a maximum K_c value ($K_{c\ max}$) is first calculated following Eq. (72) of Allen et al. (1998):

$$K_{c\ max} = \max((1.2 + (0.04(u_2 - 2) - 0.004(RH_{min} - 45)) * (h/3)^{0.3}), (K_{cb} + 0.05)) \quad (12)$$

Where u_2 is wind speed at two m above ground level, RH_{min} is daily minimum relative humidity, and h is crop height.

Next, the fraction of exposed and wetted soil (f_{ew}) is calculated following Eq. (75) of Allen et al. (1998):

$$f_{ew} = \min(1 - f_c, f_w) \quad (13)$$

Where f_w is fraction of the surface that is wetted by irrigation or precipitation. For micro-irrigation (i.e., drip irrigation or micro-jets), where most of the wetted soil is shaded, the calculation is modified as:

$$f_{ew} = \min(1-f_c, (1 - 0.67 * f_c) * f_w) \quad (14)$$

The evaporation reduction coefficient (K_r) is calculated after Eq. (74) of Allen et al. (1998):

$$K_r = (TEW - D_{e,i-1}) / (TEW - REW) \quad (15)$$

Where TEW is total evaporable water, and REW is readily evaporable water. K_r is set to 1 when $D_{e,i-1} < REW$ (evaporation is still at the maximum, or energy-limited stage). Finally, K_e is calculated after Eq. (71) of Allen et al. (1998):

$$K_e = \min(K_r * (K_{c\,max} - K_{cb}), (f_{ew} * K_{c\,max})) \quad (16)$$

K_e is set to zero for fields on subsurface irrigation (9" or deeper), except following precipitation events.

Bare-soil evaporation (E) is calculated as:

$$E = Ke * ETo \quad (17)$$

D_e is then updated on a daily timestep following Eq. (77) of Allen et al. (1998):

$$D_e = D_{e,i-1} - (P - RO) - I/f_w + E/f_{ew} \quad (18)$$

Where $D_{e,i-1}$ is D_e on the prior day, P is precipitation from events exceeding 20% of ET_o, I is irrigation depth, and RO is runoff. Runoff is calculated following Eqs. 10-11 of Part 630 Hydrology, National Engineering Handbook (USDA-NRCS, 2004) using CN=75 from Table 9-1 of the Handbook (as a compromise between row crops and orchards), using soil group B (moderate infiltration rate), "good" hydrologic condition (factors encourage infiltration), and "average" ARC (antecedent runoff condition). In addition, the S value is set to 3.33 from Handbook Eq. 10-12, and a threshold value of P=0.67 inches is needed to trigger RO.

The evaporation reduction coefficient (K_r) is calculated after Eq. (74) of Allen et al. (1998):

$$K_r = (TEW - D_{e,i-1}) / (TEW - REW) \quad (19)$$

Where TEW is total evaporable water, and REW is readily evaporable water. K_r is set to 1 when $D_{e,i-1} < REW$ (evaporation is still at the maximum, or energy-limited stage). Finally, K_e is calculated after Eq. (71) of Allen et al. (1998):

$$K_e = \min(K_r * (K_{c\,max} - K_{cb}), (f_{ew} * K_{c\,max})) \quad (20)$$

K_e was set to zero for wetting due to irrigation for fields on subsurface irrigation 9" or deeper, where it is assumed the soil surface remains dry at all times unless precipitation is observed.

K_s represents the effect of water stress on crop transpiration. K_s is minimal when the rootzone is wet (after irrigation or rainfall), and increases toward a maximum value of 1 as drainage and ET reduce the plant available water in the rootzone. For this study, a rootzone water balance model was used to derive K_s on a daily timestep. At the start of the analysis period, rootzone depletion (D_r) was initialized following Eq. (87) of Allen et al. (1998):

$$D_r = 1000 * (\theta * FC - \theta_r) * Z_r \quad (21)$$

Where θ_r is the initial water content of the rootzone, and Z_r is the depth of the rootzone. θ_r is derived by scaling the range between FC and wilting point (WP) by an initial depletion factor (α) based on the initial soil wetness. For each day thereafter in the analysis period, D_r is then calculated using Eq. (85) of Allen et al. (1998):

$$D_r = D_{r,i-1} – (P - RO) – I + ET_c \quad (22)$$

Where $D_{r,i-1}$ is the depletion on the prior day, P is the total daily precipitation, RO is runoff, I is total applied irrigation and ET_c is the crop evapotranspiration as described above. The stress coefficient, Ks, is then calculated following Eq. (84) of Allen et al. (1998):

$$K_s = (TAW - D_r) / ((1 - p) * TAW) \quad (23)$$

Where TAW is total available water after Eq. (82) of Allen et al. (1998), and p is the fraction of rootzone depletion that can occur prior to water stress onset, per Table 22 of FAO56 (Allen et al., 1998).

In the final step, $ET_{c\text{-}SIMS+}$ was calculated from the K_s, SIMS K_{cb}, K_e, and ET_o values using Eq. (9) above.

Calculation of the K_e and K_s coefficients used in the calculation of $ET_{c\text{-}SIMS+}$ incorporated site-specific information for each study field. Soil texture information for each site was obtained from the SoilWeb online soil database (O'Geen et al., 2017). Initial soil wetness was set using soil moisture measurements obtained using the instrumentation described below. The irrigation method was specified for each site, and for sites that used sprinklers for crop establishment and then switched to drip irrigation, the changeover date from sprinkler to drip irrigation was set based on irrigation records kept for each site. Daily total precipitation and irrigation were

measured for each site as described below under Section 3.3, ‘Measurement of ET via surface water balance instrumentation’.

Acknowledgements and Funding:

Development of SIMS was supported by the NASA Applied Sciences Program (NNX12AD05A), the California State University Agricultural Research Institute, and the California Department of Water Resources Water Use Efficiency Program (Award #4600010427).

References:

Abatzoglou, J. T., 2013. Development of gridded surface meteorological data for ecological applications and modelling. International Journal of Climatology, 33(1), 121-131.

Ahmad, M.U.D., Turral, H., Nazeer, A., 2009. Diagnosing irrigation performance and water productivity through satellite remote sensing and secondary data in a large irrigation system of Pakistan. Agricultural Water Management, 96(4), 551-564.

Akbari, M., Toomanian, N., Droogers, P., Bastiaanssen, W., Gieske, A., 2007. Monitoring irrigation performance in Esfahan, Iran, using NOAA satellite imagery. Agricultural Water Management, 88(1-3), 99-109.

Allen, R.G., Pereira, L.S., Raes, D., Smith, M., 1998. Crop evapotranspiration. Guidelines for computing crop water requirements. FAO Irrigation. and drainage paper 56. FAO, Rome, 300 p. (also accessible at http://www.fao.org/docrep/x0490e/x0490e00.htm)

Allen, R.G., Pereira, L.S., Smith, M., Raes, D., Wright, J.L., 2005a. FAO56 dual crop coefficient method for estimating evaporation from soil and application extensions. Journal of irrigation and drainage engineering, 131(1), 2-13.

Allen, R.G., Tasumi, M., Morse, A., Trezza, R., 2005b. A Landsat-based energy balance and evapotranspiration model in Western US water rights regulation and planning. Irrigation and Drainage systems, 19(3-4), 251-268.

Allen, R.G., Pruitt, W.O., Raes, D., Smith, M., Pereira, L.S., 2005c. Estimating evaporation from bare soil and the crop coefficient for the initial period using common soils information. Journal of irrigation and drainage engineering, 131(1), 14-23.

Allen, R.G., Tasumi, M., Morse, A., Trezza, R., Wright, J.L., Bastiaanssen, W., Kramber, W., Lorite, I., Robison, C.W., 2007. Satellite-based energy balance for mapping evapotranspiration with internalized calibration (METRIC)—Applications. Journal of irrigation and drainage engineering, 133(4), 395-406.

Allen, R. G., & Pereira, L. S., 2009. Estimating crop coefficients from fraction of ground cover and height. Irrigation Science, 28(1), 17-34.

Allen, R.G., and C.W. Robison. 2009. Evapotranspiration and Consumptive Irrigation Water Requirements for Idaho. University of Idaho Report, 222 p. Available at http://www.kimberly.uidaho.edu/ETIdaho/ (accessed 11 November 2019).

Allen, R., Irmak, A., Trezza, R., Hendrickx, J.M., Bastiaanssen, W., Kjaersgaard, J., 2011. Satellite-based ET estimation in agriculture using SEBAL and METRIC. Hydrological Processes, 25(26), 4011-4027.

Allen, R.G., Burnett, B., Kramber, W., Huntington, J., Kjaersgaard, J., Kilic, A., Kelly, C., Trezza, R., 2013. Automated calibration of the metric-landsat evapotranspiration process. JAWRA Journal of the American Water Resources Association, 49(3), 563-576.

Anderson, M. C., J. M. Norman, G. R. Diak, W. P. Kustas, J. R. Mecikalski, 1997. A two-source time-integrated model for estimating surface fluxes using thermal infrared remote sensing. Remote Sens. Environ., 60, 195–216.

Anderson, M.C., Norman, J.M., Mecikalski, J.R., Otkin, J.A., Kustas, W.P., 2007. A climatological study of evapotranspiration and moisture stress across the continental United States based on thermal remote sensing: 1. Model formulation. Journal of Geophysical Research: Atmospheres, 112(D10).

Anderson, M.C., Hain, C., Wardlow, B., Pimstein, A., Mecikalski, J.R., Kustas, W.P., 2011. Evaluation of drought indices based on thermal remote sensing of evapotranspiration over the continental United States. Journal of Climate, 24(8), 2025-2044.

Anderson, M. C., Allen, R. G., Morse, A., Kustas, W. P., 2012. Use of Landsat thermal imagery in monitoring evapotranspiration and managing water resources. Remote Sensing of Environment, 122, 50-65.

Anderson, M.C., Kustas, W.P., Hain, C.R., Cammalleri, C., Gao, F., Yilmaz, M.T., Mladenova, I.E., Otkin, J., Schull, M., Houborg, R., 2013. Mapping surface fluxes and moisture conditions from field to global scales using ALEXI/DisALEXI. Remote Sensing of Energy Fluxes and Soil Moisture Content, 207-232.

Bastiaanssen, W.G., Menenti, M., Feddes, R.A., Holtslag, A.A.M., 1998. A remote sensing surface energy balance algorithm for land (SEBAL). 1. Formulation. Journal of hydrology, 212, 198-212.

Bausch, W.C., Neale, C.M., 1987. Crop coefficients derived from reflected canopy radiation: a concept. Transactions of the ASAE, 30(3), 703-0709.

Beamer, J.P., Huntington, J.L., Morton, C.G., Pohll, G.M., 2013. Estimating annual groundwater evapotranspiration from phreatophytes in the great basin using Landsat and flux tower measurements. JAWRA Journal of the American Water Resources Association, 49(3), 518-533.

Boryan, C., Yang, Z., Mueller, R., Craig, M., 2011. Monitoring US agriculture: the US department of agriculture, national agricultural statistics service, cropland data layer program. Geocarto International, 26(5), 341-358.

Cahn, M., Johnson, L., Benzen, S., Murphy, L., Lockhart, T., Zaragosa, I., 2017. Optimizing water use of romaine lettuce using an evapotranspiration based method, Proceedings of the ASCE-EWRI World Environmental & Water Resource Congress, 21-25 May, Sacramento.

Cahn, M., R. Smith, T. Hartz, B. Farrara, L. Johnson, Melton, F., 2014. Irrigation and nitrogen management decision support tool for cool season vegetables and berries. Proceedings, USCID Water Management Conference, pp. 53-64, U.S. Committee on Irrigation & Drainage, 4-7 March, Sacramento.

Cahn, M. D., Johnson, L.F., 2018. New approaches to irrigation scheduling of vegetables, Special issue: Refining irrigation strategies in horticultural production. Horticulturae 3, 28; 10.3390/horticulturae3020028

California Department of Water Resources, 2012. A proposed methodology for quantifying the efficiency of agricultural water use. Report to the California Legislature pursuant to Section 10608.64 of the California Water Code. Available at: https://water.ca.gov/LegacyFiles/wateruseefficiency/sb7/docs/AgWaterUseReport-FINAL.pdf, (accessed 30 March 2020).

Cammalleri, C., Anderson, M.C., Gao, F., Hain, C.R., Kustas, W.P., 2013. A data fusion approach for mapping daily evapotranspiration at field scale. Water Resources Research, 49(8), 4672-4686.

Castellvi, F., Martínez-Cob, A., Pérez-Coveta, O., 2006. Estimating sensible and latent heat fluxes over rice using surface renewal. Agricultural and forest meteorology, 139(1-2), 164-169.

Castellví, F., Snyder, R.L., Baldocchi, D.D., 2008. Surface energy-balance closure over rangeland grass using the eddy covariance method and surface renewal analysis. agricultural and forest meteorology, 148(6-7), 1147-1160.

Castellví, F., Snyder, R.L., 2010. A new procedure based on surface renewal analysis to estimate sensible heat flux: a case study over grapevines. Journal of Hydrometeorology, 11(2), 496-508.

Diffenbaugh, N.S., Swain, D.L., Touma, D., 2015. Anthropogenic warming has increased drought risk in California. Proceedings of the National Academy of Sciences, 201422385.

Faunt, C. C., Sneed, M., 2015. Water availability and subsidence in California's Central Valley. San Francisco Estuary and Watershed Science, 13(3).

Fisher, J.B., Tu, K.P., Baldocchi, D.D., 2008. Global estimates of the land–atmosphere water flux based on monthly AVHRR and ISLSCP-II data, validated at 16 FLUXNET sites. Remote Sensing of Environment, 112(3), 901-919.

Fisher, J.B., Melton, F., Middleton, E., Hain, C., Anderson, M., Allen, R., McCabe, M.F., Hook, S., Baldocchi, D., Townsend, P.A., Kilic, A., 2017. The future of evapotranspiration: Global requirements for ecosystem functioning, carbon and climate feedbacks, agricultural management, and water resources. Water Resources Research, 53(4), 2618-2626.

Gee, G.W., Newman, B.D., Green, S.R., Meissner, R., Rupp, H., Zhang, Z.F., Keller, J.M., Waugh, W.J., Van der Velde, M., Salazar, J., 2009. Passive wick fluxmeters: Design considerations and field applications. Water Resources Research, 45(4), 1-18.

Glenn, E.P., Neale, C.M., Hunsaker, D.J., Nagler, P.L., 2011. Vegetation index-based crop coefficients to estimate evapotranspiration by remote sensing in agricultural and natural ecosystems. Hydrological Processes, 25(26), 4050-4062.

Goward, S.N., Markham, B., Dye, D.G., Dulaney, W., Yang, J., 1991. Normalized difference vegetation index measurements from the Advanced Very High Resolution Radiometer. Remote sensing of environment, 35(2-3), 257-277.

Griffin, D., Anchukaitis, K.J., 2014. How unusual is the 2012–2014 California drought? Geophysical Research Letters, 41(24), 9017-9023.

Gonzalez-Dugo, M. P., Neale, C. M. U., Mateos, L., Kustas, W. P., Prueger, J. H., Anderson, M. C., Li, F., 2009. A comparison of operational remote sensing-based models for estimating crop evapotranspiration. Agricultural and Forest Meteorology, 149(11), 1843-1853.

Gorelick, N., Hancher, M., Dixon, M., Ilyushchenko, S., Thau, D., Moore, R., 2017. Google Earth Engine: Planetary-scale geospatial analysis for everyone. Remote Sensing of Environment, 202, 18-27.

Guzman, A., 2018. Supporting advances in agricultural sustainability through integration of NASA SIMS and CropManage for irrigation management support. In AGU Fall Meeting Abstracts 2018 Dec.

Hart, Q. J., Brugnach, M., Temesgen, B., Rueda, C., Ustin, S. L., Frame, K., 2009. Daily reference evapotranspiration for California using satellite imagery and weather station measurement interpolation. Civil Engineering and Environmental Systems, 26(1), 19-33.

Huntington, J.L., R. Allen. 2010. Evapotranspiration and Net Irrigation Water Requirements for Nevada, Nevada State Engineer's Office Publication, 266 p. Available at http://water.nv.gov/Evapotranspiration.aspx (accessed 05 April 2020).

Johnson, L.F., Cahn, M., Martin, F., Melton, F., Benzen, S., Farrara, B., Post, K., 2016. Evapotranspiration-based irrigation scheduling of head lettuce and broccoli. HortScience, 51(7), 935-940.

Johnson, L., F. Cassel-Sharma, D. Goorahoo, Melton, F., 2014. Calculator for Evaluation of Crop Water Use Fractions in California. In AGU Fall Meeting Abstracts 2014 Dec (#H41E-0868).

Johnson, L. F., Trout, T. J., 2012. Satellite NDVI assisted monitoring of vegetable crop evapotranspiration in California's San Joaquin Valley. Remote Sensing, 4(2), 439-455.

Johnson, D.M., Mueller, R., 2010. The 2009 Cropland Data Layer. PE&RS, Photogrammetric Engineering & Remote Sensing, 76(11), 1201-1205.

Konikow, L.F., 2015. Long-term groundwater depletion in the United States. Groundwater, 53(1), 2-9.

Kustas, W.P., Anderson, M.C., Alfieri, J.G., Knipper, K., Torres-Rua, A., Parry, C.K., Hieto, H., Agam, N., White, A., Gao, F., McKee, L., 2018. The grape remote sensing atmospheric profile and evapotranspiration eXperiment (GRAPEX). Bulletin of the American Meteorological Society, 99(9), 1791-1812.

Li, H., Zheng, L., Lei, Y., Li, C., Liu, Z., Zhang, S., 2008. Estimation of water consumption and crop water productivity of winter wheat in North China Plain using remote sensing technology. Agricultural Water Management, 95(11), 1271-1278.

Linquist, B., Snyder, R., Anderson, F., Espino, L., Inglese, G., Marras, S., Moratiel, R., Mutters, R., Nicolosi, P., Rejmanek, H., Russo, A., 2015. Water balances and evapotranspiration in water-and dry-seeded rice systems. Irrigation science, 33(5), 375-385.

Lund, J., Medellin-Azuara, J., Durand, J., Stone, K., 2018. Lessons learned from California's 2012-2016 Drought. Journal of Water Resources Planning and Management, 144(10),

Mann, M.E., Gleick, P.H., 2015. Climate change and California drought in the 21st century. Proceedings of the National Academy of Sciences, 112(13), 3858-3859.

McElrone, A.J., Shapland, T.M., Calderon, A., Fitzmaurice, L., Snyder, R.L., 2013. Surface renewal: an advanced micrometeorological method for measuring and processing field-scale energy flux density data. JoVE (Journal of Visualized Experiments), (82), p.e50666.

Medellín-Azuara, J., et al., 2018. Estimation of Crop Evapotranspiration in the Sacramento-San Joaquin Delta. Report from the University of California at Davis, available at: https://watershed.ucdavis.edu/project/delta-et (accessed 01 November 2019)

Melton, F., Johnson, L., Lund, C., Pierce, L., Michaelis, A, Guzman, A., Trout, T., Temesgen, B., Frame, K., Sheffner, E., and Nemani, R. Satellite Mapping of Crop Condition and ET for Irrigation Management Support. IEEE J-STARS, special issue on Interoperability Architectures and Arrangements for Multi-Disciplinary Earth Observation Systems. IEEE J. of Selected Topics in Applied Earth Observations and Remote Sensing, 5(6), 1709-1721.

Morton, C.G., Huntington, J.L., Pohll, G.M., Allen, R.G., McGwire, K.C. and Bassett, S.D., 2013. Assessing calibration uncertainty and automation for estimating evapotranspiration from agricultural areas using METRIC. JAWRA Journal of the American Water Resources Association, 49(3), 549-562.

Mu, Q., Zhao, M., Running, S.W., 2005. Brief introduction to MODIS evapotranspiration data set (MOD16). Water Resources Research, 45, 0-4.

Mu, Q., Zhao, M., Running, S.W., 2011. Improvements to a MODIS global terrestrial evapotranspiration algorithm. Remote Sensing of Environment, 115(8), 1781-1800.

Neale, C.M., Bausch, W.C. and Heermann, D.F., 1990. Development of reflectance-based crop coefficients for corn. Transactions of the ASAE, 32(6), 1891-1900.

Nagler, P., Glenn, E., Nguyen, U., Scott, R., Doody, T., 2013. Estimating riparian and agricultural actual evapotranspiration by reference evapotranspiration and MODIS enhanced vegetation index. Remote Sensing, 5(8), 3849-3871.

O'Geen, A., Walkinshaw, M. and Beaudette, D., 2017. SoilWeb: A multifaceted interface to soil survey information. Soil Science Society of America Journal, 81(4), 853-862.

Otkin, J.A., Anderson, M.C., Hain, C., Svoboda, M., 2014. Examining the relationship between drought development and rapid changes in the evaporative stress index. Journal of Hydrometeorology, 15(3), 938-956.

Paw U, K.T., Snyder, R.L., Spano, D., Su, H., 2005. Surface renewal estimates of scalar exchange. Agronomy, 47, p.455.

Pereira L.S., Paredes P., Melton F.S., Johnson L.F., López-Urrea R., Cancela J., Allen R.G., 2020. Prediction of basal crop coefficients from fraction of ground cover and height. Agric. Water Manage., Special Issue on Updates to the FAO56 Crop Water Requirements Method, (in press), https://doi.org/10.1016/j.agwat.2020.106197.

Pôças, I., Calera, A., Campos, I., Cunha, M., 2020. Remote sensing for estimating and mapping single and basal crop coefficients: A review on spectral vegetation indices approaches. Agricultural Water Management, 233, p.106081.

Rosa, R., Dicken, U., Tanny, J., 2013. Estimating evapotranspiration from processing tomato using the surface renewal technique. Biosystems engineering, 114(4), 406-413.

Samani, Z., Bawazir, A.S., Bleiweiss, M., Skaggs, R., Longworth, J., Tran, V.D., Pinon, A., 2009. Using remote sensing to evaluate the spatial variability of evapotranspiration and crop coefficient in the lower Rio Grande Valley, New Mexico. New Mexico Journal of Science, 46, 1-16.

Santos, C., Lorite, I.J., Tasumi, M., Allen, R.G., Fereres, E., 2008. Integrating satellite-based evapotranspiration with simulation models for irrigation management at the scheme level. Irrigation Science, 26(3), 277-288.

Scanlon, T.M., Kustas, W.P., 2010. Partitioning carbon dioxide and water vapor fluxes using correlation analysis. Agricultural and forest meteorology, 150(1), 89-99.

Scanlon, T.M., Kustas, W.P., 2012. Partitioning evapotranspiration using an eddy covariance-based technique: Improved assessment of soil moisture and land–atmosphere exchange dynamics. Vadose Zone Journal, 11(3).

Scanlon, B.R., Faunt, C.C., Longuevergne, L., Reedy, R.C., Alley, W.M., McGuire, V.L., McMahon, P.B., 2012. Groundwater depletion and sustainability of irrigation in the US High Plains and Central Valley. Proceedings of the national academy of sciences, 109(24), 9320-9325.

Semmens, K.A., Anderson, M.C., Kustas, W.P., Gao, F., Alfieri, J.G., McKee, L., Prueger, J.H., Hain, C.R., Cammalleri, C., Yang, Y. and Xia, T., 2016. Monitoring daily evapotranspiration over two California vineyards using Landsat 8 in a multi-sensor data fusion approach. Remote Sensing of Environment, 185, 155-170.

Senay, G.B., Bohms, S., Singh, R.K., Gowda, P.H., Velpuri, N.M., Alemu, H. and Verdin, J.P., 2013. Operational evapotranspiration mapping using remote sensing and weather datasets: A new parameterization for the SSEB approach. JAWRA Journal of the American Water Resources Association, 49(3), 577-591.

Senay, G.B., Friedrichs, M., Singh, R.K., Velpuri, N.M., 2016. Evaluating Landsat 8 evapotranspiration for water use mapping in the Colorado River Basin. Remote Sensing of Environment, 185, 171-185.

Shapland, T.M., Snyder, R.L., Smart, D.R., Williams, L.E., 2012. Estimation of actual evapotranspiration in winegrape vineyards located on hillside terrain using surface renewal analysis. Irrigation science, 30(6), 471-484.

Shapland, T.M., McElrone, A.J., Snyder, R.L., 2013. A turnkey data logger program for field-scale energy flux density measurements using eddy covariance and surface renewal. Italian Journal of Agrometeorology, (1), 5-16.

Shaw, R.H., Snyder, R.L., 2003. Evaporation and eddy covariance. Encyclopedia of water science, 235-237.

Snyder, R.L., Bali, K., Ventura, F., Gomez-MacPherson, H., 2000. Estimating evaporation from bare or nearly bare soil. J. of irrigation and drainage engineering, 126(6), 399-403.

Swinbank, W.C., 1951. The measurement of vertical transfer of heat and water vapor by eddies in the lower atmosphere. J. Meteorol, 8, 135–145.

Trout, T.J., Johnson, L.F., Gartung, J., 2008. Remote sensing of canopy cover in horticultural crops. HortScience, 43(2), 333-337.

USDA, 2018. Census of Agriculture Irrigation and Water Management Survey, Table 23: Methods Used in Deciding When to Irrigate. Available online at:

https://www.nass.usda.gov/Publications/AgCensus/2017/Online_Resources/Farm_and_Ranch_Irrigation_Survey/fris_1_0023_0023.pdf, (accessed 14 April 2020).

USDA-NRCS, 2004. National Engineering Handbook Hydrology, Chapters 9, 10, available at: http://www.nrcs.usda.gov/wps/portal/nrcs/detailfull/national/water/?cid=stelprdb1043063, (accessed 14 April 2020).

Vinukollu, R.K., Wood, E.F., Ferguson, C.R., Fisher, J.B., 2011. Global estimates of evapotranspiration for climate studies using multi-sensor remote sensing data: Evaluation of three process-based approaches. Remote Sensing of Environment, 115(3), 801-823.

Wolf, A., Saliendra, N., Akshalov, K., Johnson, D.A., Laca, E., 2008. Effects of different eddy covariance correction schemes on energy balance closure and comparisons with the modified Bowen ratio system. Agricultural and forest meteorology, 148(6-7), 942-952.

Zwart, S.J., Bastiaanssen, W.G., 2007. SEBAL for detecting spatial variation of water productivity and scope for improvement in eight irrigated wheat systems. Agricultural water management, 89(3), 287-296.